

Accepted Manuscript

Title: Nanotextured gold coatings on carbon nanofiber scaffolds as ultrahigh surface-area electrodes

Authors: Kevin. M. Metz, Paula E. Colavita, Kiu-Yuen Tse, Robert J. Hamers



PII: S0378-7753(11)01934-3
DOI: doi:10.1016/j.jpowsour.2011.09.098
Reference: POWER 14915

To appear in: *Journal of Power Sources*

Received date: 3-8-2011
Revised date: 28-9-2011
Accepted date: 28-9-2011

Please cite this article as: Kn.M. Metz, P.E. Colavita, K.-Y. Tse, R.J. Hamers, Nanotextured gold coatings on carbon nanofiber scaffolds as ultrahigh surface-area electrodes, *Journal of Power Sources* (2010), doi:10.1016/j.jpowsour.2011.09.098

This is a PDF file of an unedited manuscript that has been accepted for publication. As a service to our customers we are providing this early version of the manuscript. The manuscript will undergo copyediting, typesetting, and review of the resulting proof before it is published in its final form. Please note that during the production process errors may be discovered which could affect the content, and all legal disclaimers that apply to the journal pertain.

- High density edge plane containing carbon nanofibers electrodes are modified
- Electroless metal deposition is used to deposited highly textured gold coatings
- The electrochemical response of the hybrid electrodes is characterized
- The modified electrodes hold promise for varied applications in energy storage

Accepted Manuscript

1 Nanotextured gold coatings on carbon 2 nanofiber scaffolds as ultrahigh surface-area 3 electrodes

4
5 Kevin. M. Metz^{1*}, Paula E. Colavita², Kiu-Yuen Tse³, and Robert J. Hamers
6 Department of Chemistry, University of Wisconsin-Madison, 1101 University Ave.,
7 Madison, WI 53706, USA
8

9 **Keywords**

10 Gold
11 Carbon
12 Electrodes
13 Nanoscale
14 Supercapcitor
15

16 **Abstract**

17 High surface area metal electrodes are desirable for applications in energy storage
18 and energy conversion. Here, the formation and electrochemical characterization of a
19 hybrid material made by electroless deposition of gold onto a scaffolding of vertically
20 aligned carbon nanofibers is described. Vertically aligned carbon nanofibers, ~80 nm in
21 diameter, provided mechanical support and electrical contact to the highly textured
22 nanoscale gold coatings. By chemically functionalizing the nanofiber surfaces and then
23 using electroless deposition methods, a highly textured metal coating was formed. The
24 electrochemical response of these “nano-on-nano” hybrid electrodes was characterized
25 using electrochemical methods. The results show that using the metallic coatings can
26 increase the electrochemically active surface area by up to a factor of 10 compared with

* Corresponding author. Tel.: 1 517-629-0656; fax: 1-517-629-0264. E-mail address: kmetz@albion.edu

¹ Present address: Department of Chemistry, Albion College, 611 E. Porter St., Albion, MI 49224, USA

² Present address: School of Chemistry, Trinity College Dublin, College Green, Dublin 2, Ireland

³ Present address: 3M Company, Corporate Research Materials Laboratory, St Paul, MN 55144-1000, USA

27 the starting carbon nanofiber scaffolds. The electrochemical response of the electrodes
28 was modulated by varying the deposition time of the gold.

29

30 **1. Introduction**

31 Recently high surface area materials, such as nano-composites, have received
32 much attention as substrates for emerging energy storage and conversion technologies[1-
33 3] associated with supercapacitors[4, 5], next-generation batteries[6], fuel cells [7-9], and
34 catalysis [10, 11]. Nanoscale forms of carbon, including nanotubes and nanofibers, have
35 been the focus of much research due to their excellent chemical stability and electrical
36 conductivity [2, 3]. Nanoscale forms of carbon can also be combined with polymers or
37 metals to form nano-composites [3, 7, 9, 12-16]. Such nano-composites are attractive
38 because their properties can be altered, building from the excellent performance of the
39 nanoscale carbon to create structures with tailored chemical or electrical properties [2, 3].
40 However, fabrication of these composites can be hampered by the atomic perfection of
41 nanoscale carbon, which can create non-reactive surfaces. For example, many types of
42 nanoscale carbon need to be oxidized before metals can be deposited [13]. Often, the
43 oxidation processes used are harsh and can damage, or destroy, much of the carbon.
44 Additionally, accessibility of the full surface area can be difficult to achieve.

45 A gold-carbon nanocomposite based on vertically aligned carbon nanofibers
46 (VACNFs) [17] has previously been reported on. The fabrication method takes advantage
47 of the fact that nanofibers can be grown in a structure in which graphene sheets are nested
48 inside one another in a stacked-cup arrangement. This structure exposes large amounts of
49 edge-plane graphite along the sidewalls. Photochemical functionalization of the

50 nanofibers with a molecular layer exposing carboxylic acid groups leads to extremely
51 efficient nucleation of metals onto the nanofibers [17, 18]. The use of photochemical
52 functionalization has the advantage of being fully compatible with metal substrates and
53 causing no damage to the physical properties of the nanofibers.

54 Previous studies also showed that metal deposition on top of the molecular
55 monolayer modified VACNFS increased the active area of the electrode by a factor of ten
56 compared to the nanofiber template; creating an electrode with a 100 fold increase in
57 electrochemically accessible surface area compared to a planar electrode [17].
58 Additionally, it was demonstrated that the effective capacitance of these highly textured
59 electrodes scaled with the accessible surface area [17].

60 Here a more thorough characterization of Faradaic and non-Faradaic response of
61 these highly textured, nano-structured gold electrodes in order to understand the resulting
62 interfacial electrical response. Data that helps elucidate the mechanism of the electroless
63 plating on molecular monolayer-modified carbon surfaces is presented. Additionally, the
64 electrical response of the electrodes at the interface of aqueous solution, both in the
65 presence and absence of electron transfer reagents, is investigated. Finally, comparisons
66 are made to other types of high surface area electrodes. The results demonstrate that
67 metal-on-carbon hybrid nanostructures, which have a high surface capacitance and lower
68 contact resistance, can provide very high surface area of electrochemically accessible,
69 chemically stable materials that may be of potential utility in energy storage, e.g., as
70 electrodes in electrochemical double layer capacitors [4].

71

72 **2. Experimental**

73 *2.1 Growth of carbon nanofibers.*

74 Carbon nanofibers were grown in a custom built chamber using DC plasma
75 enhanced chemical vapor deposition (DC-PECVD) [19-21]. Silicon substrates (with their
76 native oxide) were coated with 50 nm of molybdenum, 20 nm of titanium, and 20 nm
77 nickel as the top layer. Nanofibers were grown using acetylene and ammonia with flow
78 rates of 30 standard cubic centimeters per minute (sccm) and 80 sccm, respectively, at a
79 chamber pressure of 4 Torr and a DC power of 360 W. Growth times and conditions
80 determine the physical properties of the nanofibers produced. Here, all fibers were
81 grown for 15 minutes, which produces high densities of vertically aligned, cylindrical
82 nanofibers with an average diameter of 80 nm and an average length of 2 μm .

83
84 *2.2 Gold deposition on carbon nanofibers.*

85 To enhance nucleation of gold the nanofibers were functionalized with a
86 molecular monolayer in order to produce a high density of carboxylic acid groups along
87 the nanofiber sidewalls. This was achieved using a photochemical grafting procedure
88 developed previously [22] in which organic molecules bearing a terminal alkene group
89 (C=C) covalently grafts to the graphitic edge-planes of VACNFs when illuminated with
90 ultraviolet light at 254 nm [23]. This method has been shown to form molecular layers
91 that allow facile electron transport [24]. Here, this work is extended to metallic layers on
92 carbon nanofibers. Freshly grown VACNFs were reacted with undecylenic acid methyl
93 ester by dripping a thin film of the pure liquid reagent onto the VACNF samples, and
94 illuminating with 254 nm light ($\sim 1 \text{ mW cm}^{-2}$) for 16-18 hours in a nitrogen-purged
95 reaction chamber. The surface-linked ester was then converted to carboxylic acid using a

96 slurry of potassium tert-butoxide in dimethyl sulfoxide [24], producing carbon nanofibers
97 functionalized with carboxylic acid moieties. The fibers were then cleaned in 0.1 M HCl
98 and washed in a 50:50 solution of distilled water and methanol.

99 Deposition of gold onto the COOH-terminated nanofibers [17] was achieved by
100 sensitizing the carboxylic acid-modified fibers in a bath containing 0.026 M SnCl₂ and
101 0.07 M trifluoroacetic acid in a 50:50 methanol: deionized water solution; this step binds
102 tin ions to the carboxylic acid moieties on the surface [25]. The tin sensitized fibers
103 were then activated with silver by immersion in a silver bath consisting of 0.03 M
104 ammoniacal silver nitrate. This leaves atomic silver bound to the surface, via a redox
105 reaction with the tin ions. Finally the VACNF samples were placed in individual gold
106 baths, containing 0.127 M Na₂SO₃, 0.025 M NaHCO₃, 0.625 M formaldehyde and 8 mM
107 Na₃Au(SO₃)₂ (Technic Oromerse Part B gold solution), at pH 10, and 6°C for durations
108 of 1 to 22 hours. The time in the gold bath controlled the amount of gold on the fibers
109 [17].

111 2.3 Electrical characterization.

112 Electrical characterization was carried out using electrochemical impedance
113 spectroscopy (EIS) and Cyclic Voltammetry (CV) using a three-electrode geometry.
114 Measurements were made in aqueous solutions of KCl, KClO₄, and Ru(NH₃)₆^{+2/+3}, of
115 various concentrations. All measurements used the gold-coated carbon nanofiber sample
116 as the working electrode. For comparison, capacitance measurements were made in
117 aqueous solutions of KCl over planar gold and glassy carbon electrodes. The data were
118 collected using a single junction Ag/AgCl (3M KCl) reference electrode. In all

119 measurements ohmic contact was made to the top side of the gold-coated carbon
120 nanofiber samples outside of the fluid compartment of the cell. Impedance
121 measurements were made at the open circuit potential in room temperature. Aqueous
122 solutions were purged with argon prior to use. All data shown here have been normalized
123 to the geometric area of the cells used. All measurements were performed using a 3-
124 electrode potentiostat and impedance analyzer (Solartron 1260/1287) using Zplot or
125 Corrware software (Scribner Associates, Inc).

126

127 *2.4 Fourier Transform Infrared (FTIR) Measurements.*

128 The chemical functionalization and tin sensitization of the carbon nanofibers were
129 verified using infrared spectroscopy. Spectra were collected using infrared reflection
130 absorption spectroscopy (IRRAS) in a Bruker Vertex 70 FTIR spectrometer with a
131 variable angle reflection accessory (VeeMaxII, Pike). Spectra shown here were collected
132 with *s*-polarized light at an incidence angle of 60° from the surface normal. The
133 background and sample spectra each consisted of 500 scans at 4 cm⁻¹ resolution. Spectra
134 were baseline-corrected using commercial software (Grams, Thermo Galactic).

135

136 **3. Results**

137 *3.1 Nanoscale morphology.*

138 Figure 1 shows scanning electron microscope (SEM) images of as-grown
139 VACNFs before any modification (Figure 1A) and functionalized nanofibers after
140 immersion in the gold deposition bath for different lengths of time. It is clear from Figure
141 1A that the fibers are cylindrical, vertically aligned and packed in a high density

142 arrangement. Once functionalized and placed in a gold bath, nanoparticles of gold
143 nucleate and grow on the carbon nanofibers. Figure 1B shows VACNFs after 3 hours in
144 a gold bath. At this point the nanoparticles are clearly visible and in some cases have
145 started to coalesce. After 5 hours in the gold bath the gold nanoparticles have fully
146 coalesced, forming a textured gold sheath that completely encapsulates the carbon
147 nanofibers. With continued time in the gold bath, the gold sheath forms a more complex
148 texture, with spike-like features frequently extending more than 100 nm long. Figure 1C
149 shows a gold-carbon composite after 7 hours in a gold bath, which displays this complex,
150 highly textured gold coating. The interactions of the spike-like projections on
151 neighboring fibers form a very complex, essentially random network in the interstitials
152 between the fibers.

153 Control experiments were performed on planar carbon surfaces that were
154 functionalized with an identical monolayer. The functionalized planar surfaces showed a
155 high density of nanocrystalline gold particles and some regions of spongy masses of gold,
156 but did not show the complex morphology observed on the functionalized VACNFs.

157

158 *3.2 Characterization of functionalization chemistry and impact on electroless deposition*
159 *on VACNF electrodes.*

160 An important aspect of the fabrication method is the use of a molecular layer to
161 provide carboxylic acid sites for metal binding. Infrared spectroscopy was used to
162 characterize the chemical changes associated with the functionalization and their
163 influence on the final structures shown in Figure 1. Figure 2 shows infrared absorption
164 spectra of carbon nanofibers that were photochemically functionalized and de-protected

165 to expose carboxylic acid groups before(Figure 2A) and after (Figure 2B) exposure to
166 tin. Figure 2C shows a control spectrum for a carbon nanofiber sample that was not
167 functionalized, but was exposed to the tin sensitization bath. The absorption band of
168 atmospheric carbon dioxide near 2360 cm^{-1} has been omitted for clarity. All spectra were
169 collected and referenced to a background spectrum collected from a freshly grown, bare
170 carbon nanofiber sample using a 60° incidence angle and s-polarized light.

171 All three spectra are dominated by a large peak near 1587 cm^{-1} ; this peak appears
172 to originate in C=C binding vibrations of the bulk nanofibers and thus is related to the
173 nanofiber structure. Therefore examination of changes in the weaker features in the
174 spectra is needed to monitor changes in the surface chemistry. The FTIR spectrum shown
175 in trace (A) of Figure 2 shows methylene (CH_2) peaks at 2927 and 2856 cm^{-1} and a sharp
176 peak in the C=O regions at 1715 cm^{-1} [26].

177 The importance of surface chemical termination is revealed more clearly after the
178 next step of functionalization, which involves binding of tin as a sensitizer to the
179 nanofibers. Tin exposure was carried out by wetting the fibers with methanol and then
180 soaking them in the tin sensitizing bath for 30 minutes. The spectrum of the “bare”
181 nanofibers that was exposed to tin shows no significant features other than the peak near
182 1587 cm^{-1} , which corresponds to the bulk nanofibers. For the COOH-modified samples
183 (Fig. 2b), exposure to tin leads to no significant change in the C-H region, but the peak at
184 1715 cm^{-1} (2A) disappears and is replaced with a new peak at 1658 cm^{-1} (2B). This is
185 very close to the value of 1655 cm^{-1} previously reported for the C=O antisymmetric
186 stretching of tin carboxylate [27].

187 The FTIR data show that (1) photochemical functionalization leads to formation
188 of stable monolayers, and (2) that immersion into the tin bath leads to clear, well-defined
189 changes in the spectra corresponding with the transition from –COOH termination to –
190 $(\text{COO}^-)_2\text{Sn}^{+2}$. Finally, the fact that no significant CO features are observed on the “bare”
191 nanofibers either before (data not shown) or after tin treatment demonstrates that the bare
192 nanofibers have only small numbers of carboxylic acid groups, below the detection limit
193 of FTIR. The fact that there is no corresponding peak in the bare nanofibers spectrum
194 provides direct evidence that the molecular layer is needed to create oxidized carbon sites
195 for metal binding (*vide infra*).

196

197 3.3 Electrochemical impedance measurements.

198 Electrochemical impedance spectroscopy (EIS) was used to examine how the
199 evolution in morphology from the simple cylinders to the more complex geometry visible
200 in Figure 1 alters the electrical properties of the interface. In EIS, a small modulation
201 with a root-mean-square (RMS) amplitude of ~ 10 mV is applied to the sample. The in-
202 phase and out-of-phase components of the current are measured, and the impedance is
203 described by the complex quantity

$$204 \quad Z = Z' + iZ'' \quad (1)$$

205 Impedance data are usually presented as plots of the magnitude ($|Z|$) and phase angle (θ)
206 of the impedance as a function of frequency. Figure 3 shows EIS on bare carbon
207 nanofibers and on carboxylic acid-modified nanofibers that were exposed to the gold
208 electroless deposition bath for 3 hours and 7 hours. These measurements were made in
209 0.1 M KCl solution at the open circuit potential (0.086 V, 0.023 V, and 0.044 V vs.

210 Ag/AgCl for the bare, 3 h and 7 h samples respectively). At low frequencies, all three
211 samples show nearly linear decreases in impedance, dropping over the range from 0.1 Hz
212 to 10 Hz. Figure 3A shows that increased time in the gold bath results in a lower
213 impedance at low frequency. At 0.1 Hz, the lowest frequency measured here, the
214 absolute impedance drops from $\sim 2600 \Omega \text{ cm}^2$ for bare nanofibers, through $\sim 820 \Omega \text{ cm}^2$
215 for nanofibers with gold deposited 3 hours to a minimum of $\sim 400 \Omega \text{ cm}^2$ for nanofibers
216 with 7 hours of gold deposition, representing a ratio of impedances of $\sim 1.0 : 0.31 : 0.15$.
217 This ratio of impedances is over the frequency range from 0.1 Hz to 10-100 Hz. At high
218 frequency, greater than 1 kHz, the area-normalized impedance of all three samples drops
219 to a few $\Omega \text{ cm}^2$. This impedance corresponds to the uncompensated resistance of the
220 solution. While this uncompensated resistance should be the same for all samples, some
221 variations arise due to slight irreproducibility in the position of the reference electrode, as
222 verified by independent control experiments.

223 Figure 3B shows that increased time in the gold bath also results in a larger phase
224 angle. A phase angle of -90° corresponds to ideal capacitance, whereas a phase angle of
225 0° corresponds to pure resistance. All three samples show roughly sigmoidal shaped
226 curves as a function of frequency. Bare nanofibers and 3 hour gold-coated nanofibers
227 show a phase angle of approximately -60° at 0.1 Hz while nanofibers with 7 hours of gold
228 deposited on them show a phase angle of -74° . All three curves shift upwards, towards -
229 90° , before falling to near 0° at frequencies around 1 kHz. This higher phase angle
230 observed at low frequency implies that with the addition of more gold, the fibers become
231 slightly more ideally capacitive.

232 The formation of the highly textured gold surfaces is accompanied by a change in
233 the electrode material (carbon to gold) and in the effective area in contact with the
234 electrolyte solution. In the case of carbon based electrodes, the capacitance further
235 depends on the ratio of basal-plane to edge-plane graphite present [28, 29]. To help
236 determine how each of these factors contributes to the changes in impedance, EIS
237 measurements were made on planar glassy carbon and planar gold electrodes in 0.1 M
238 KCl solutions. Glassy carbon was selected as planar comparison because it contains a
239 large amount of edge-plane graphite [30], much akin to the carbon nanofibers.

240 Figure 4 shows the impedance and phase angle vs. frequency for these samples.
241 At the lowest frequencies (0.1 Hz) the impedances for gold and glassy carbon samples
242 are both substantially larger than those observed with nanofiber samples. In both cases,
243 the total impedance drops nearly linearly from 0.1 Hz to $\sim 10^2$ - 10^3 Hz, and at higher
244 frequencies plateaus at a constant value corresponding to the uncompensated solution
245 resistance. The phase angle data, Figure 4B, again exhibit roughly sigmoidal shapes,
246 reaching phase angles of -80° at the lowest frequency, increasing very slightly toward
247 90° , and then at a frequency of 10^2 - 10^3 Hz dropping toward zero. Figure 4A shows that
248 the glassy carbon electrodes display approximately twice the impedance of the gold
249 sample. This difference likely arises from a combination of factors including an increased
250 density of states and higher roughness for the gold sample and indicates that the much
251 more pronounced difference observed in comparing bare VANCFs with gold-covered
252 VACNFs is primarily geometric in origin, but may have some contribution from the
253 difference in materials

254 Another possible contributor to the absolute impedance observed with the
255 addition of gold to carbon nanofibers is the high specific adsorption of chloride ions to
256 gold [31]. To help separate the effects of surface area and specific adsorption,
257 experiments were performed changing the composition and concentration of the
258 electrolyte concentration. Since potassium perchlorate (KClO_4) does not exhibit strong
259 adsorption to gold [32], data in chloride- and perchlorate-containing solutions can be
260 used to assess whether there is strong specific adsorption to the gold surfaces. Figure 5
261 shows absolute impedance and phase angle data for gold coated carbon nanofibers in 0.1
262 M KCl and 0.1 M KClO_4 measured at the open circuit potential. The spectra in Figure 5
263 are not significantly different from one another; this demonstrates that the impedance
264 behavior of the Au-coated fibers is not dominated by anion adsorption effects.

265

266 *3.4 Charge transfer at electrodes.*

267 To determine how the nanotextured gold coating impacts the electron-transfer
268 properties of the sample, Faradaic processes at the surfaces using the redox couple
269 $\text{Ru}(\text{NH}_3)_6^{2+/3+}$ were examined. Previous studies have shown that $\text{Ru}(\text{NH}_3)_6^{2+/3+}$ is an
270 outer-sphere system involving electron transfer that is sensitive primarily to the density of
271 states of the electrode, and relatively insensitive to surface chemical composition [33].
272 Figure 6 shows the magnitude and phase of the impedance measured on an electrode with
273 gold deposited on it for 7 hours in 0.1 M KCl, and in a solution of 0.1 M KCl with 5 mM
274 each of $\text{Ru}(\text{NH}_3)_6^{2+}$ and $\text{Ru}(\text{NH}_3)_6^{3+}$, collected at the open circuit potential. A fit to an
275 equivalent circuit model, is also shown. The equivalent circuit used to construct this fit is
276 shown in Figure 6C, and consists of a resistor, modeling the solution resistance, in series

277 with the parallel combination of a CPE and a resistor, which model the capacitance and
278 charge transfer at the interface. The parameters used in the modeling are presented in
279 table 1.

280 Figure 6A shows that above ~100 Hz, the presence of the redox agent has no
281 significant change on the electrical response. At lower frequencies, however, the
282 magnitude of the impedance is reduced. For example at 0.1 Hz the absolute impedance
283 decreases from ~400 to ~100 $\Omega \text{ cm}^2$. The phase angle response (Figure 6B) takes on a
284 new shape in the presence of the redox couple, changing from the roughly sigmoidal
285 shape observed in 0.1 M KCl to a more linear response at low frequency, falling from
286 about -45° at 0.1 Hz to roughly 0° at 100 Hz. This is consistent with the fact that the
287 impedance at these frequencies is limited by the uncompensated solution resistance,
288 which is mostly unchanged by the addition of a low concentration of redox couple to the
289 0.1 M KCl solution.

290 As a point of reference, Figure 7 shows impedance and phase angle data for
291 planar glassy carbon and gold electrodes in 0.1 M KCl and in 0.1 M KCl containing 5
292 mM each of $\text{Ru}(\text{NH}_3)_6^{2+}$ and $\text{Ru}(\text{NH}_3)_6^{3+}$, measured at the OCP. Figure 7 shows that,
293 much akin to the behavior of the gold-modified carbon nanofibers, the addition of a redox
294 couple significantly lowers the absolute impedance and phase angle of the planar
295 electrodes at low frequency. However, the effect is much more dramatic with the planar
296 samples. For example, at 0.1 Hz the hexaamineruthenium complex causes the impedance
297 of the glassy carbon electrode to decrease from ~173 $\text{k}\Omega \text{ cm}^2$ to ~150 $\Omega \text{ cm}^2$ and the
298 impedance of the gold electrode to drop from ~18 $\text{k}\Omega \text{ cm}^2$ to ~150 $\Omega \text{ cm}^2$.

299 One of the most significant results from these studies is that while for planar
300 electrodes the redox agent reduces the impedance by a factor of more than 100, on gold-
301 coated nanofibers the reduction is much smaller. This implies that the high surface area
302 of the nanofibers is not the limiting factor in the Faradaic processes.

303 To explore the kinetics under quasi-steady state conditions, Figure 8 shows cyclic
304 voltammograms of gold coated carbon nanofibers (Figure 8A) and a planar gold
305 electrode (Figure 8B) in a solution of 5 mM each of $\text{Ru}(\text{NH}_3)_6^{2+/3+}$ with 0.1 M KCl, at a
306 scan rate of 25 mVs^{-1} . The shapes of the curves are different near the most positive and
307 most negative potentials. This shape difference arises from the capacitance charging of
308 the surface during the measurement. Figure 8B also shows a peak current nearly twice as
309 large as Figure 8A, however calculating the area from the peak current, after removing
310 the capacitive current contribution, results in the geometric area of the cell used here.
311 This indicates that the gold coated nanofibers are in a planar diffusion regime. Diffusion
312 effects may also be responsible for the increased peak separation. It is reasonable that
313 diffusion effects seem to dominate given the very complex, nearly random networks that
314 exist between the individual fibers.

315

316 **4. Discussion**

317 *4.1 Materials requirements for metal-nanofiber composites.*

318 Recent studies have emphasized that high surface area, well-defined porosity and
319 high crystallinity are indispensable requirements for materials in many energy storage
320 and conversion applications [9]. For metals, high crystallinity implies good conductivity,

321 and the high surface area with well-defined porosity implies a highly accessible surface
322 area.

323 Previous studies on high surface area porous carbon have shown that the very
324 small pores, which lead to high surface area, are not always accessible and can have
325 difficulty supporting well defined electrical double layers [5]. Carbon nanotubes and
326 nanofibers have emerged as novel high surface-area materials of intense interest.
327 However, one problem with small-diameter (e.g., single-walled) carbon nanotubes is that
328 their atomic structure is based upon wrapping of graphene sheets in such a manner that
329 they expose almost entirely basal-plane graphite along their sidewalls.

330 In contrast, nanofibers grown by the methods used here expose large amounts of
331 edge-plane graphite. In nanocarbons, such as single walled nanotubes and nanofibers, the
332 activity is often increased by harsh oxidation procedures such as boiling in hot nitric acid,
333 which creates defects and partially oxidizes the materials [13].

334 Another approach to increasing the surface area is to use nanostructures as a
335 template for other materials, such as metals. This is particularly attractive for
336 applications such as electrocatalysis, where the high surface area and tunable chemical
337 reactivity of the metals can both be used. However, the results demonstrate that even
338 noble metals such as gold can provide significant increases in the accessible surface area
339 that could be used to practical advantage. VACNFs have been shown to increase the
340 surface area of an electrode by at least 7 times [34]. This results from the well defined
341 cylindrical geometry that VACNFs assume. Each fiber in a VACNF electrode also has
342 the added benefit of an individual contact to the underlying electrode as a result of the
343 growth mechanism. Thus VACNFs by themselves meet the requirements for materials

344 applications in energy storage and conversion, making them an ideal choice for
345 modifications.

346

347 *4.2 Surface modification.*

348 One key issue in forming metal nanocomposites on carbon surfaces is the
349 adhesion of the metals to the carbon surface. This is typically enhanced by oxidation of
350 the surface using strong oxidizing acids, such as HNO₃. While this procedure can be
351 effective, especially for bulk high surface-area carbons, it also has a few drawbacks.
352 First, wet-chemical oxidation leads to a broad distribution of different types of oxidized
353 carbon, only some of which are effective at binding to metals. This can be problematic
354 for nanostructured carbon materials. Secondly, the harsh oxidizers are difficult to
355 integrate with many metals commonly used as electrode materials. In contrast, the FTIR
356 data show that the molecular functionalization with only carboxylic acid moieties was
357 achieved on the surface under extremely gentle conditions, using 254 nm light to trigger
358 the reaction.

359 One issue of initial concern was whether the molecules would act as insulators,
360 adding a series resistance to the nanofiber-metal interface. However, the results suggest
361 that any such resistances are negligible. These results are also consistent with previous
362 results [34-36] using several different molecules, in each case showing that although the
363 molecular densities are relatively high, the layers are sufficiently porous that good
364 electrical contact is still made between the nanofiber and the metal electrode. Thus, the
365 molecular monolayer can be used to enhance metal adhesion to the nanofibers without
366 adversely affecting the electrical properties.

367

368 *4.3 Surface texture.*

369 While the use of molecular monolayers provides a high density of chelating sites
370 for metal deposition, the electroless deposition process results in a surprisingly
371 corrugated surface texture. Electroless metal deposition generally results in smooth films
372 [37]. Textured structures similar to those reported here have been reported previously
373 from electrochemical deposition onto highly-oriented pyrolytic graphite (HOPG) [38-40],
374 with dendritic gold nanoparticles nucleating at step edges of the HOPG. Steps on HOPG
375 reveal atomic structures essentially identical to those of the edge planes exposed every
376 ~2-3 nm along the VACNFs.

377 In these previous studies, the highly textured geometry has been attributed to
378 anisotropic diffusion of gold on different crystal planes, which can depend strongly on
379 the types of ions in solution. Similar spike-like coatings, or dendritic coatings, can be
380 formed by electroless deposition, but usually only under fast deposition conditions. That
381 is, conditions of high pH, elevated temperatures, or large metal concentrations [41-43].
382 Under these conditions the deposition reactions are fast and diffusion limited aggregation
383 generally dominates the growth, resulting in a more fractal looking structure [42, 43].

384 The method reported here is not operating under these conditions. Similar
385 electroless gold deposition protocols used on porous polymer surfaces [25, 44, 45], as
386 well as planar polymer and glass surfaces [46] have not reported any spike-like textures
387 with their deposits. Additionally, control experiments performed in on planar glassy
388 carbon, using identical procedures as described above, did not result in any highly
389 textured deposits. While the formation of this highly textured coating remains not fully

390 understood, it appears that the highly textured coating leads to many of the observed
391 electrochemical properties of the electrodes.

392

393 *4.4 Electrochemical behavior of the textured surface.*

394 Understanding the electrochemical behavior of gold surface is essential to
395 understanding and predicting the response of the electrodes. Electrodes of this nature
396 generally are either treated as rough electrodes and described by distributed elements
397 such as a constant phase element (CPE) [47], or they are treated as porous electrodes and
398 described with a transmission line model (TLM) [48], in which the impedance of a pore
399 is defined in terms of an infinitely long transmission line defined by the solution
400 resistivity and the impedance of the wall-electrolyte interface [48-50]. The distinction as
401 to which of these two models is most appropriate is based on the depth of the pores
402 relative to an effective penetration depth that describes how far an AC electric field
403 penetrates into the pores [48-50]. The depth of the “pores” is $\sim 2 \mu\text{m}$. In this size range,
404 the TLM model collapses to a rough electrode model [49] and a simple distributed
405 element, such as a constant-phase element, is a better choice than the TLM for modeling
406 the electrical properties of the system [47].

407 The CPE is defined via the impedance relationship $Z_{\text{cpe}} = 1/T(i\omega)^\phi$, where T and ϕ
408 are parameters. A perfect capacitor has $T=C$ and $\phi=1$; deviations from these values can
409 reflect a variety of non-ideal properties including microscopic roughness, electrical
410 inhomogeneities at the interface, or diffusion limits to the electrode [47, 51, 52]. An
411 electrode that shows deviations based solely on diffusion limited effects has an exponent
412 equal to 0.5 [52]; exponents between 0.5 and 1 are often attributed to roughness effects

413 [47, 51]. It is likely that the complex shape of the electrodes leads to a combination of
414 these effects.

415 Table 1 summarizes the parameters determined by fitting the data with an
416 equivalent circuit consisting of a resistor in series with the parallel combination of a CPE
417 and a resistor. It is clear from table 1 that the samples show a significant deviation from
418 ideal capacitance ($\phi=1$). If the electrodes were behaving as true porous systems with
419 diffusion occurring primarily between fibers down the length of the pore, one would
420 expect an exponent value of 0.5 [52]. Diffusion occurring between a rough surface and
421 the solution should result in an exponent between 0.5 and 1 [47, 51]. Thus, the exponent
422 of 0.88 obtained for the gold-coated nanofiber electrodes in 0.1 M KCl implies that the
423 microscopic surface roughness associated with the network of gold influences the
424 response of the electrodes, rather than diffusion between individual fibers in this system.
425 Table 1 also shows that when the electrolyte concentration is kept constant but a redox
426 agent is added, the charge-transfer resistance drops significantly, and the exponent value
427 changes from 0.88 to 0.59. This change in the exponential value suggests a transition
428 from complex behavior to more diffusion limited behavior in the presence of a redox
429 agent, given that exponential values of 0.5, generally indicate diffusion limited behavior.

430 Calculations of active surface area based on the measurements in the presence of
431 a redox couple show an area equivalent to the projected area of the electrode, rather than
432 the extended area of the length of the fibers enhanced by the microtextured gold coating.
433 This supports the hypothesis that diffusion occurs primarily between the nanofibers and
434 the solution, and this limits the performance of the electrode in the presence of a redox
435 couple. It should also be pointed out that the deviation from ideal capacitive behavior

436 observed for gold coated carbon fibers is not significantly different from the deviation
437 observed for bare carbon nanofibers with no gold coating, in KCl solutions [53]. The
438 similarity in exponents between “bare” and gold-coated nanofibers implies that the
439 deviation from “ideal” behavior is associated primarily with the nanofibers and not with
440 the smaller-scale structure of the gold. This implies that the active surface area can be
441 increased, without significantly altering the frequency response of the electrode, by the
442 addition of gold in the absence of charge transfer.

443 The very high surface area provided by gold coating leads to interesting properties
444 that could potentially be useful for applications such as energy storage in electrochemical
445 double-layer capacitors[1]. Assuming a series RC model, the effective capacitance of the
446 system can be extracted from the impedance using

$$448 \quad C = \frac{-1}{2\pi f Z \sin \theta} \quad (2)$$

449
450 The high surface area obtained after 7 hours of gold deposition, leads to an effective
451 capacitance of 3.25 mF cm^{-2} [17]. This is a substantial increase compared to the average
452 effective capacitance of 290 mF cm^{-2} for bare nanofibers in the same solution [17]. The
453 value of 3.25 mF cm^{-2} is comparable to that obtained from rough porous gold electrode
454 produced by leaching out a component from a gold alloy [54]. The short nanofibers
455 investigated here yield capacitance values that are slightly smaller than the values of ~ 0.5
456 to 50 mF cm^{-2} obtained from high surface-area activated carbon electrodes in aqueous
457 solution of KOH [5, 55]. Nonetheless, the combination of highly textured gold on top of

458 carbon nanofiber scaffolding presents a unique material that can be customized for
459 different applications.

460

461 **5. Conclusions**

462 A new fabrication method for producing tunable nanoscale gold-carbon
463 composite electrodes has been demonstrated. The method utilizes molecular
464 functionalization, developed for planar carbon materials, to provide a high density of
465 carboxylic acid binding sites uniformly distributed along the length of the carbon
466 nanofiber starting materials. This approach avoids strong oxidants, making this method
467 fully compatible with metal substrates. The deposition process allows for control over
468 the amount of gold added to the surface. The resulting electrodes show high accessibility
469 in aqueous solutions. This method should be extendible to different metals, allowing for
470 the creation of electrodes for use in a variety of applications including energy conversion
471 and electrocatalysis.

472 The tunable nature of the metal deposition process can lead to useful substrate
473 materials ranging from highly disperse particles of metal [18], useful in applications such
474 as fuel cells and catalysis, to the full, highly textured coatings studied here. Gold has been
475 shown to be catalytically active when present in the nanoscale [11, 56, 57]. Nanoscale
476 gold has also attracted attention recently as a catalysis substrate for fuel cells [45, 58, 59].
477 In these applications, using a small amount of metal does not significantly alter the
478 electrical response of the underlying carbon nanofibers [18]. Thus this method could be
479 used to fabricate metal-coated carbon nanofibers with varied amounts of metal,
480 depending on the needs of the study and/or application.

481 In addition to the tunable metal coating, this approach is also flexible in terms of
482 geometry and scale. While this approach was demonstrated here on vertically aligned
483 carbon nanofibers grown on an electrode, free standing carbon nanofibers with high
484 densities of edge plane carbon are commercially available. Given the availability of such
485 materials, scaling up this approach and using varied geometries should be possible. There
486 are several functionalization methods that can be used to add molecular monolayers to
487 free standing carbon nanofibers[60], creating the anchoring sites for metal deposition.
488 Coupling these methods with electroless deposition, as demonstrated here, will create a
489 highly flexible materials platform useful in many varied applications.

490

491 **Acknowledgments**

492 This work was supported in part by the National Science Foundation Grant DMR-
493 0210806.

494

495 **References**

- 496 [1] A.S. Arico, P. Bruce, B. Scrosati, J.M. Tarascon, W. Van Schalkwijk, *Nat. Mater.*, 4
497 (2005) 366-377.
- 498 [2] R. Baughman, A. Zakhidov, W. de Heer, *Science*, 297 (2002) 787-792.
- 499 [3] P.J.F. Harris, *Int. Mater. Rev.*, 49 (2004) 31-43.
- 500 [4] P. Sharma, T.S. Bhatti, *Energy Conversion and Management*, 51 (2010) 2901-2912.
- 501 [5] E. Frackowiak, F. Beguin, *Carbon*, 39 (2001) 937-950.
- 502 [6] J. Chen, F.Y. Cheng, *Acc. Chem. Res.*, 42 (2009) 713-723.

- 503 [7] E.S. Steigerwalt, G.A. Deluga, C.M. Lukehart, *J. Phys. Chem. B*, 106 (2002) 760-
504 766.
- 505 [8] E.S. Steigerwalt, G.A. Deluga, D.E. Cliffel, C.M. Lukehart, *J. Phys. Chem. B*, 105
506 (2001) 8097-8101.
- 507 [9] C. Kim, Y.J. Kim, Y.A. Kim, T. Yanagisawa, K.C. Park, M. Endo, M.S. Dresselhaus,
508 *J. Appl. Phys.*, 96 (2004) 5903-5905.
- 509 [10] M.D. Hughes, Y.J. Xu, P. Jenkins, P. McMorn, P. Landon, D.I. Enache, A.F. Carley,
510 G.A. Attard, G.J. Hutchings, F. King, E.H. Stitt, P. Johnston, K. Griffin, C.J. Kiely,
511 *Nature*, 437 (2005) 1132-1135.
- 512 [11] M. Valden, X. Lai, D.W. Goodman, *Science*, 281 (1998) 1647-1650.
- 513 [12] S. Arai, M. Endo, S. Hashizume, Y. Shimojima, *Electrochem. Commun.*, 6 (2004)
514 1029-1031.
- 515 [13] Z.L. Liu, X.H. Lin, J.Y. Lee, W. Zhang, M. Han, L.M. Gan, *Langmuir*, 18 (2002)
516 4054-4060.
- 517 [14] X.C. Ma, X. Li, N. Lun, S.L. Wen, *Mater. Chem. Phys.*, 97 (2006) 351-356.
- 518 [15] Z.Q. Tian, S.P. Jiang, Y.M. Liang, P.K. Shen, *J. Phys. Chem. B*, 110 (2006) 5343-
519 5350.
- 520 [16] H. Vu, F. Goncalves, R. Philippe, E. Lamouroux, M. Corrias, Y. Kihn, D. Plee, P.
521 Kalck, *P. Serp, J. Catal.*, 240 (2006) 18-22.
- 522 [17] K.M. Metz, K.Y. Tse, S.E. Baker, E.C. Landis, R.J. Hamers, *Chem. Mater.*, 18
523 (2006) 5398-5400.
- 524 [18] K.M. Metz, D. Goel, R.J. Hamers, *J. Phys. Chem. C*, 111 (2007) 7260-7265.

- 525 [19] Y. Chen, Z.L. Wang, J.S. Yin, D.J. Johnson, R.H. Prince, *Chem. Phys. Lett.*, 272
526 (1997) 178-182.
- 527 [20] A.V. Melechko, V.I. Merkulov, T.E. McKnight, M.A. Guillorn, K.L. Klein, D.H.
528 Lowndes, M.L. Simpson, *J. Appl. Phys.*, 97 (2005) 041301-041339.
- 529 [21] M. Meyyappan, L. Delzeit, A. Cassell, D. Hash, *Plasma Sources Sci. Technol.*, 12
530 (2003) 205-216.
- 531 [22] S.E. Baker, K.Y. Tse, E. Hindin, B.M. Nichols, T.L. Clare, R.J. Hamers, *Chem.*
532 *Mater.*, 17 (2005) 4971-4978.
- 533 [23] E.C. Landis, K.L. Klein, A. Liao, E. Pop, D.K. Hensley, A.V. Melechko, R.J.
534 Hamers, *Chem. Mater.*, 22 2357-2366.
- 535 [24] S.E. Baker, P.E. Colavita, K.Y. Tse, R.J. Hamers, *Chem. Mater.*, 18 (2006) 4415-
536 4422.
- 537 [25] V.P. Menon, C.R. Martin, *Anal. Chem.*, 67 (1995) 1920-1928.
- 538 [26] G. Socrates, *Infrared and Raman Characteristic Group Frequencies: Tables and*
539 *Charts*, 3rd ed., John Wiley & Sons, LTD., New York, 2001.
- 540 [27] N.W. Alcock, V.M. Tracy, T.C. Waddington, *J. Chem. Soc.-Dalton Trans.*, (1976)
541 2243-2246.
- 542 [28] R.L. McCreery, *Carbon Electrodes: Structural Effects on Electron Transfer Kinetics*,
543 in: A.J. Bard (Ed.) *Electroanalytical Chemistry*, Marcel Dekker, Inc, 1990, pp. 221.
- 544 [29] R.J. Rice, R.L. McCreery, *Anal. Chem.*, 61 (1989) 1637-1641.
- 545 [30] M.T. McDermott, C.A. McDermott, R.L. McCreery, *Anal. Chem.*, 65 (1993) 937-
546 944.
- 547 [31] Z. Kerner, T. Pajkossy, *Electrochim. Acta*, 47 (2002) 2055-2063.

- 548 [32] B.D. Cahan, H.M. Villullas, E.B. Yeager, *J. Electroanal. Chem.*, 306 (1991) 213-
549 238.
- 550 [33] P.H. Chen, M.A. Fryling, R.L. McCreery, *Anal. Chem.*, 67 (1995) 3115-3122.
- 551 [34] S.E. Baker, K.Y. Tse, C.S. Lee, R.J. Hamers, *Diamond Relat. Mater.*, 15 (2006) 433-
552 439.
- 553 [35] E.C. Landis, R.J. Hamers, *J. Phys. Chem. C*, 112 (2008) 16910-16918.
- 554 [36] E.C. Landis, K.L. Klein, A. Liao, E. Pop, D.K. Hensley, A.V. Melechko, R.J.
555 Hamers, *Chem. Mater.*, 22 (2010) 2357-2366.
- 556 [37] G.O. Mallory, J.B. Hajdu, in, *American Electroplaters and Surface Finishers*
557 *Society*, Orlando, FL, 1990.
- 558 [38] C.J. Boxley, H.S. White, T.E. Lister, P.J. Pinhero, *J. Phys. Chem. B*, 107 (2003)
559 451-458.
- 560 [39] H. Martin, P. Carro, A.H. Creus, S. Gonzalez, G. Andreasen, R.C. Salvarezza, A.J.
561 Arvia, *Langmuir*, 16 (2000) 2915-2923.
- 562 [40] H. Martin, P. Carro, A.H. Creus, S. Gonzalez, R.C. Salvarezza, A.J. Arvia,
563 *Langmuir*, 13 (1997) 100-110.
- 564 [41] S.S. Djokic, *J. Electrochem. Soc.*, 144 (1997) 2358-2363.
- 565 [42] A. Kuhn, F. Argoul, *J. Electroanal. Chem.*, 397 (1995) 93-104.
- 566 [43] A. Kuhn, F. Argoul, J.F. Muzy, A. Arneodo, *Phys. Rev. Lett.*, 73 (1994) 2998-3001.
- 567 [44] M. Nishizawa, V.P. Menon, C.R. Martin, *Science*, 268 (1995) 700-702.
- 568 [45] M.A. Sanchez-Castillo, C. Couto, W.B. Kim, J.A. Dumesic, *Angew. Chem., Int. Ed.*,
569 43 (2004) 1140-1142.
- 570 [46] Z.Z. Hou, N.L. Abbott, P. Stroeve, *Langmuir*, 14 (1998) 3287-3297.

- 571 [47] T. Pajkossy, *J. Electroanal. Chem.*, 364 (1994) 111-125.
- 572 [48] J. Bisquert, G. Garcia-Belmonte, F. Fabregat-Santiago, N.S. Ferriols, P. Bogdanoff,
573 E.C. Pereira, *J. Phys. Chem. B*, 104 (2000) 2287-2298.
- 574 [49] O.E. Barcia, E. D'Elia, I. Frateur, O.R. Mattos, N. Pebere, B. Tribollet, *Electrochim.*
575 *Acta*, 47 (2002) 2109-2116.
- 576 [50] R. de Levie, *Electrochim. Acta*, 9 (1964) 1231-1245.
- 577 [51] G.J. Brug, A.L.G. Vandeneeden, M. Sluytersrehabach, J.H. Sluyters, *J. Electroanal.*
578 *Chem.*, 176 (1984) 275-295.
- 579 [52] S.R. Taylor, E. Gileadi, *Corrosion*, 51 (1995) 664-671.
- 580 [53] K.Y. Tse, L.Z. Zhang, S.E. Baker, B.M. Nichols, R. West, R.J. Hamers, *Chem.*
581 *Mater.*, 19 (2007) 5734-5741.
- 582 [54] R. Jurczakowski, C. Hitz, A. Lasia, *J. Electroanal. Chem.*, 572 (2004) 355-366.
- 583 [55] H. Shi, *Electrochim. Acta*, 41 (1996) 1633-1639.
- 584 [56] G.J. Hutchings, M. Haruta, *Appl. Catal., A*, 291 (2005) 2-5.
- 585 [57] M. Haruta, T. Kobayashi, H. Sano, N. Yamada, *Chem. Lett.*, (1987) 405-408.
- 586 [58] A.C. Gluhoi, H.S. Vreeburg, J.W. Bakker, B.E. Nieuwenhuys, *Appl. Catal., A*, 291
587 (2005) 145-150.
- 588 [59] W.B. Kim, T. Voithl, G.J. Rodriguez-Rivera, J.A. Dumesic, *Science*, 305 (2004)
589 1280-1283.
- 590 [60] R.L. McCreery, *Chem. Rev.*, 108 (2008) 2646-2687.
- 591
- 592
- 593

594

595

596

597

598

599

600 Figure Captions

601 Figure 1. Scanning electron microscopy images of carbon nanofibers A) before gold
602 bath, B) after 3 hours in a gold bath and C) after 7 hours in a gold bath.

603

604 Figure 2. Fourier transform infrared (FTIR) spectra of carbon nanofibers.

605 A) functionalized with carboxylic acids

606 B) functionalized with carboxylic acids and exposed to tin;

607 C) control sample without functionalization but exposed to tin.

608

609 Figure 3. A) Absolute impedance and B) phase angle as a function of frequency,

610 measured at the open circuit potential in 0.1 M KCl for bare carbon nanofiber

611 (dash-dotted line), carbon nanofibers after 3 h gold deposition (dotted line) and

612 carbon nanofibers after 7 h gold deposition (solid line).

613

614 Figure 4. A) Absolute impedance and B) phase angle as a function of frequency,

615 measured at the open circuit potential in 0.1 M KCl for glassy carbon (solid) and

616 gold (dotted) planar electrode

617 .

618 Figure 5. A) Absolute impedance and B) phase angle as a function of frequency,

619 measured at the open circuit potential in 0.1 M KCl (solid) 0.1 M KClO₄ (dotted)

620 on a 7 h gold-coated carbon nanofiber electrode

621

622 Figure 6. A) Absolute impedance and B) phase angles response as a function of
623 frequency for a 7 h gold- coated carbon nanofiber electrode in 100 mM KCl
624 (crosses) and in 4 mM $\text{Ru}(\text{NH}_3)_6$ in 100 mM KCl (circles). The lines represent
625 fits calculated using the C) equivalent circuit model.

626

627 Figure 7. Absolute impedance and phase angle as a function of frequency, in 0.1 M KCl
628 (crosses), and 5 mM $\text{Ru}(\text{NH}_3)_6^{2+/3+}$ in 0.1 M KCl (circles) on glassy carbon (A &
629 B) and gold (C & D) planar electrodes. Line represent fits to the data calculated
630 using the equivalent circuit model in Figure 6C.

631

632 Figure 8. Cyclic voltammograms collected in 5 mM $\text{Ru}(\text{NH}_3)_6^{2+/3+}$ in 0.1 M KCl at 25
633 mV s^{-1} over A) a planar gold electrode and B) a 7 h gold-coated carbon nanofiber
634 electrode.

635

636

637 Table 1. Equivalent circuit model (Figure 7C.) parameters for a 7 h gold-coated carbon
638 nanofiber electrode, a planar gold electrode and a planar glassy carbon electrode
639 in 0.1 M KCl and 5 mM $\text{Ru}(\text{NH}_3)_6^{2+/3+}$ in 0.1. M KCl.

640

641

642

<u>Model Component</u>	<u>Gold-CNF</u>		<u>Gold Foil</u>		<u>Glassy Carbon</u>	
	KCl	Ru ^{2+/3+}	KCl	Ru ^{2+/3+}	KCl	Ru ^{2+/3+}
R _s (Ohm)	11	12	35	32	34	33
R _{ct} (Ohm)	6.9 x 10 ³	8.1 x 10 ²	3.5 x 10 ⁶	1.6 x 10 ¹¹	3.3 x 10 ¹³	1.1 x 10 ¹¹
CPE T	0.0038	0.0129	8.7 x 10 ⁻⁵	0.01	4.1 x 10 ⁻⁵	0.01
CPE φ	0.88	0.59	0.92	0.50	0.88	0.50

Accepted Manuscript

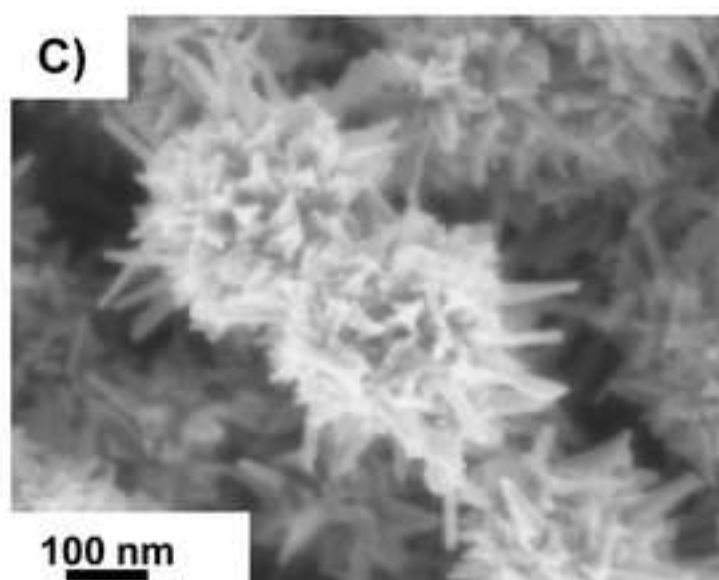
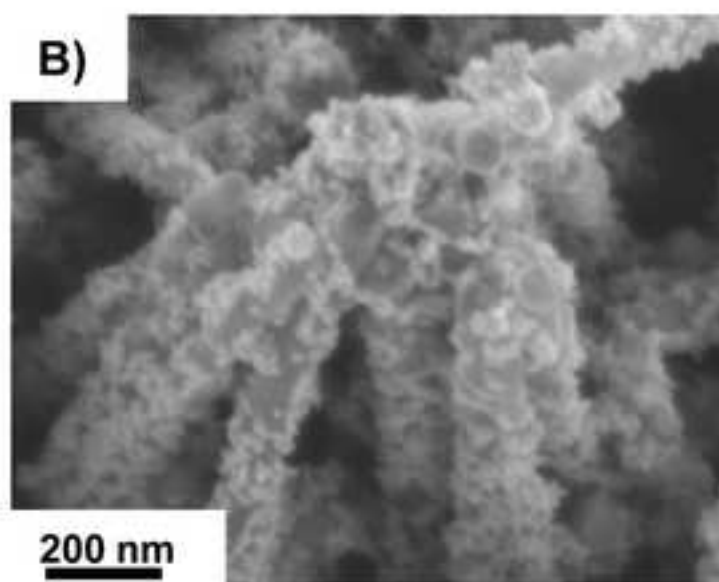
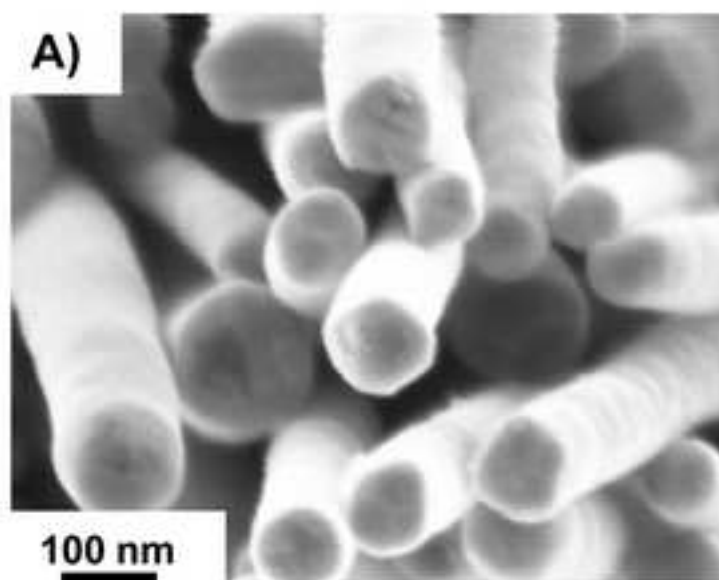
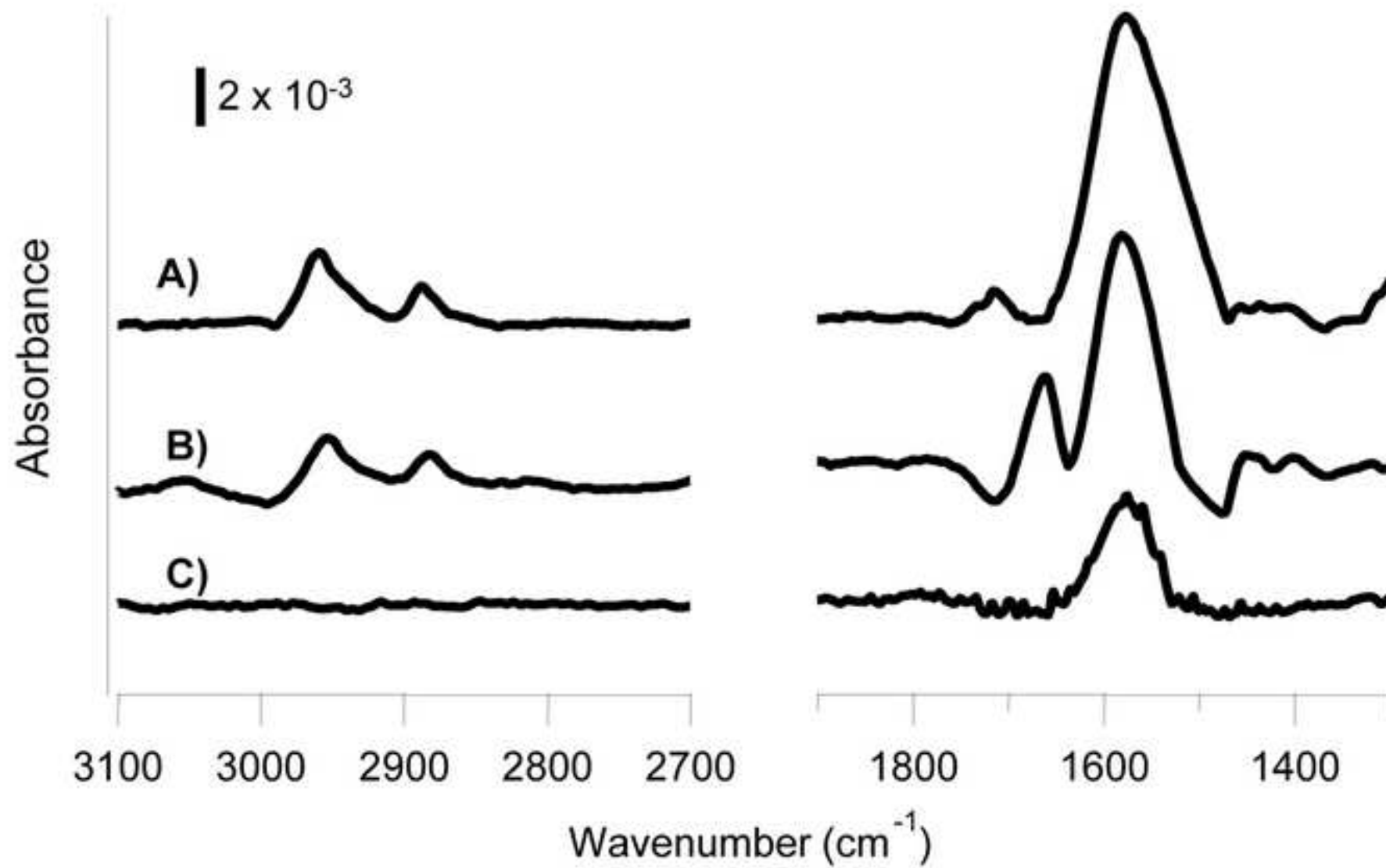
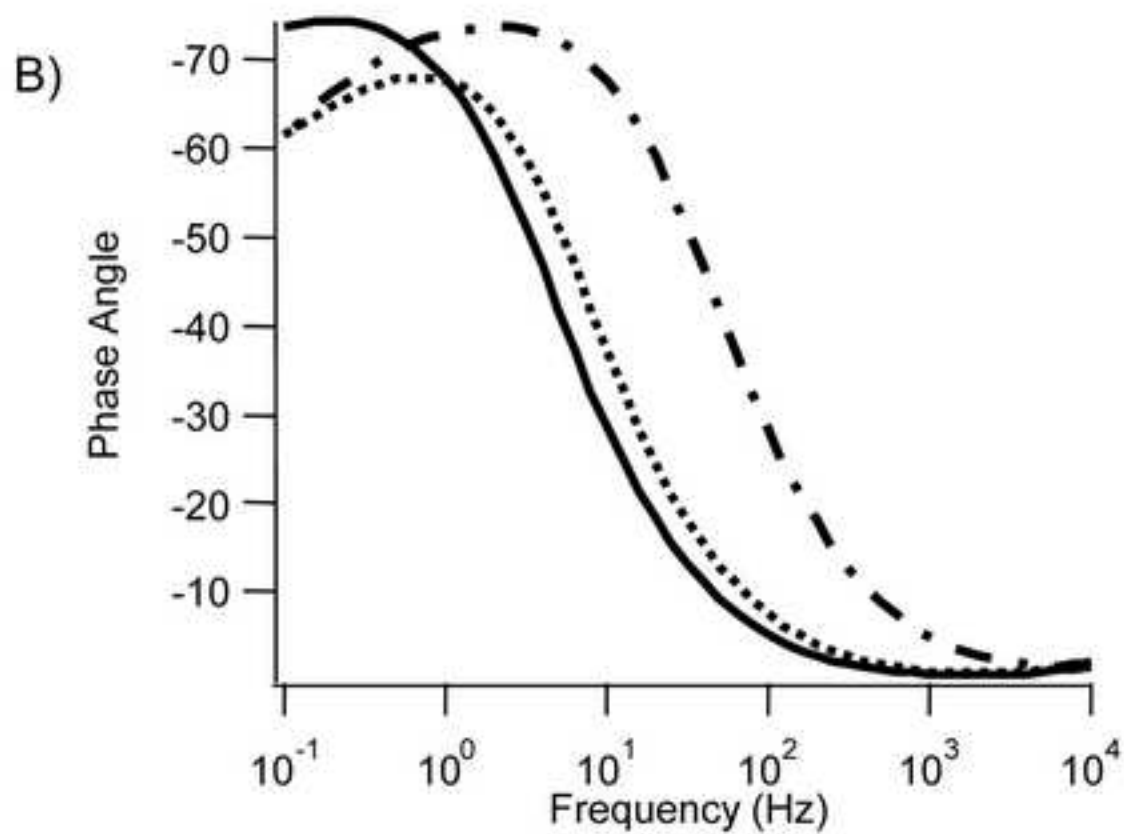
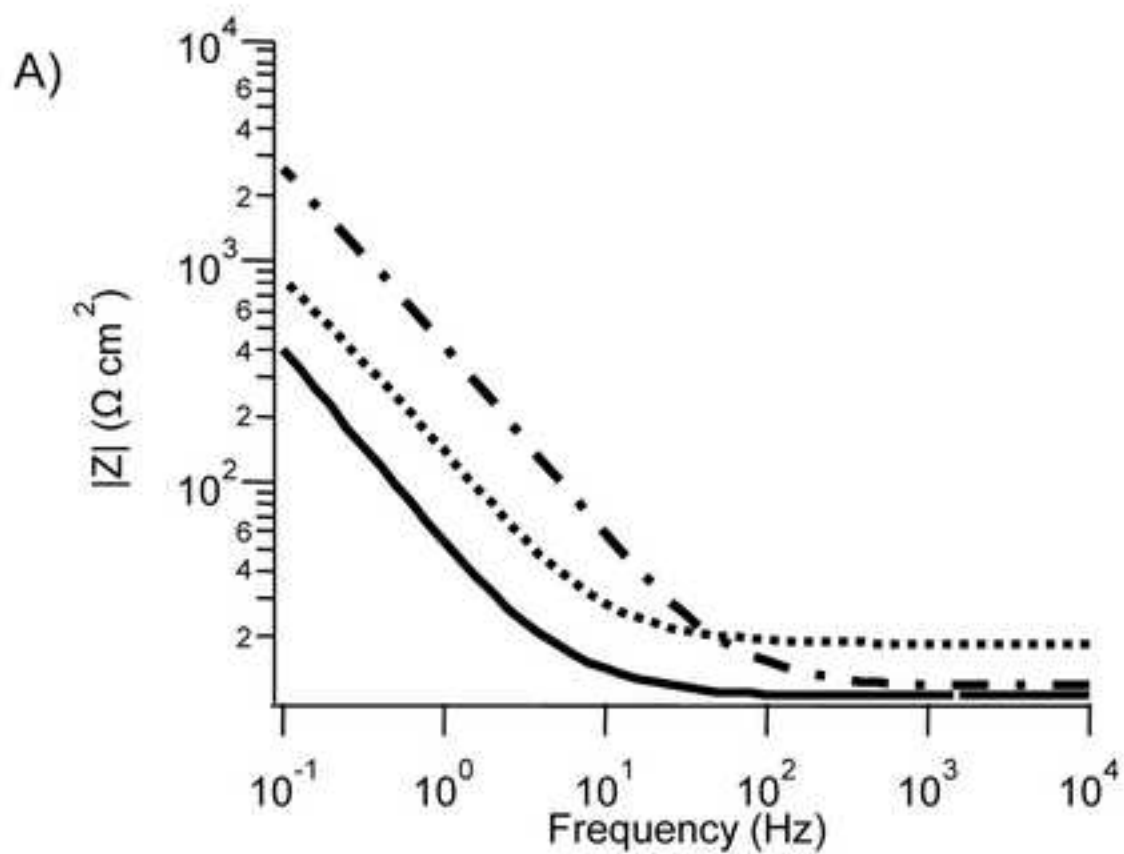
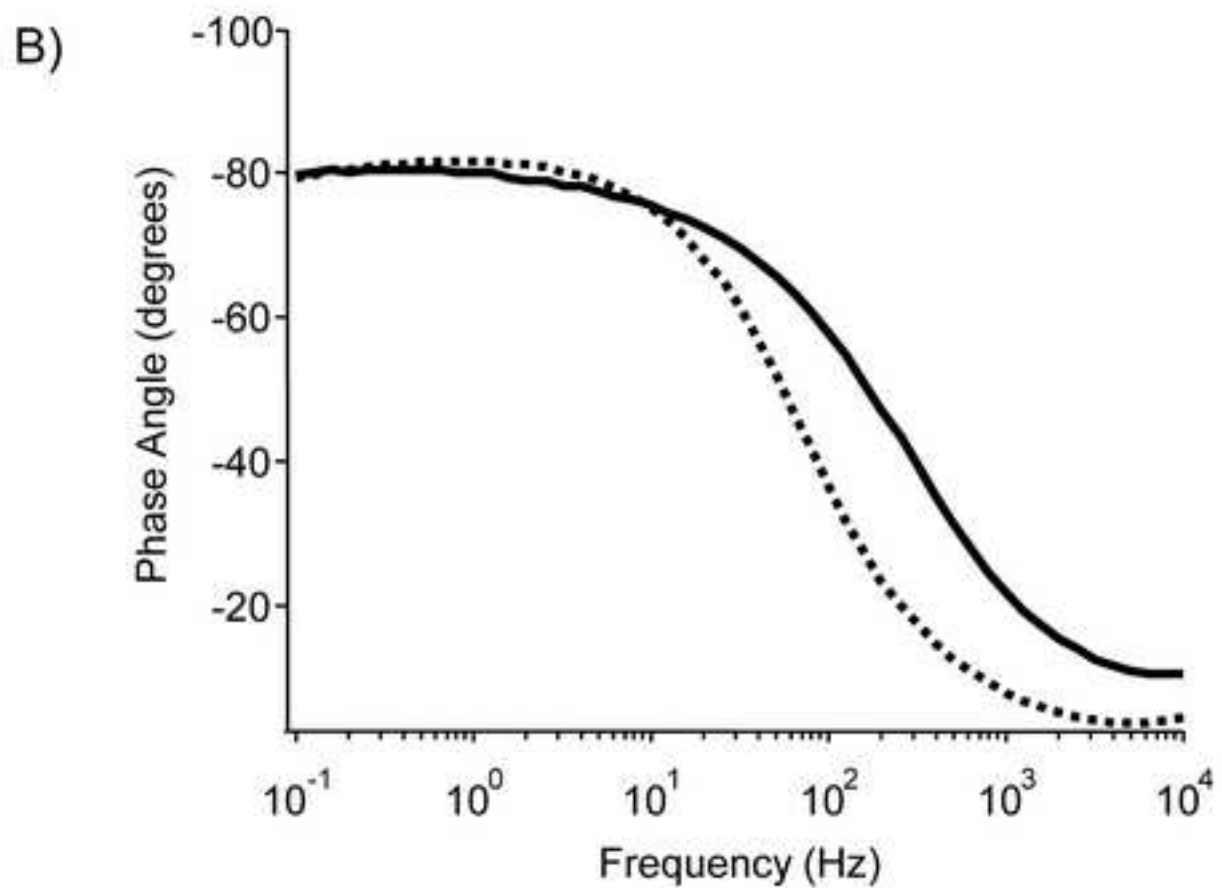
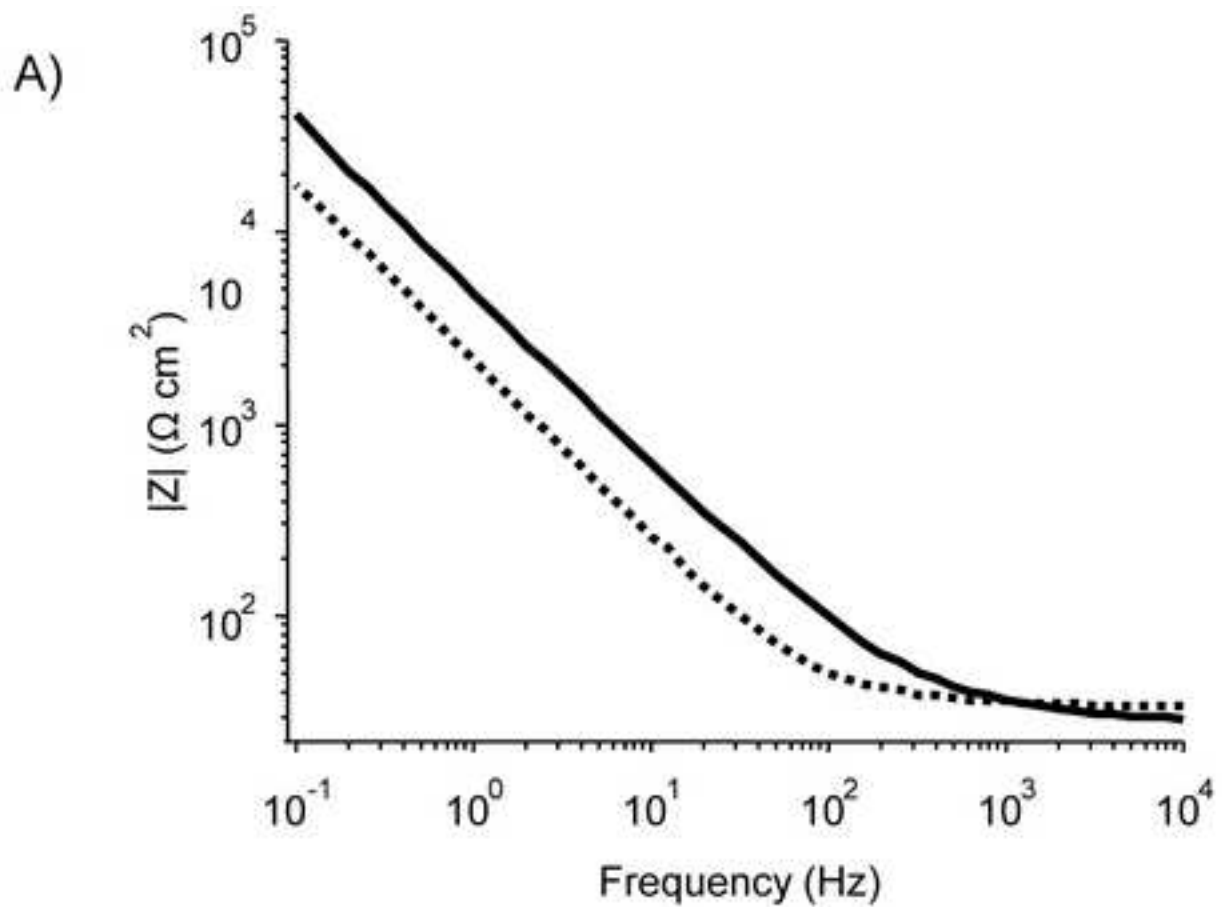
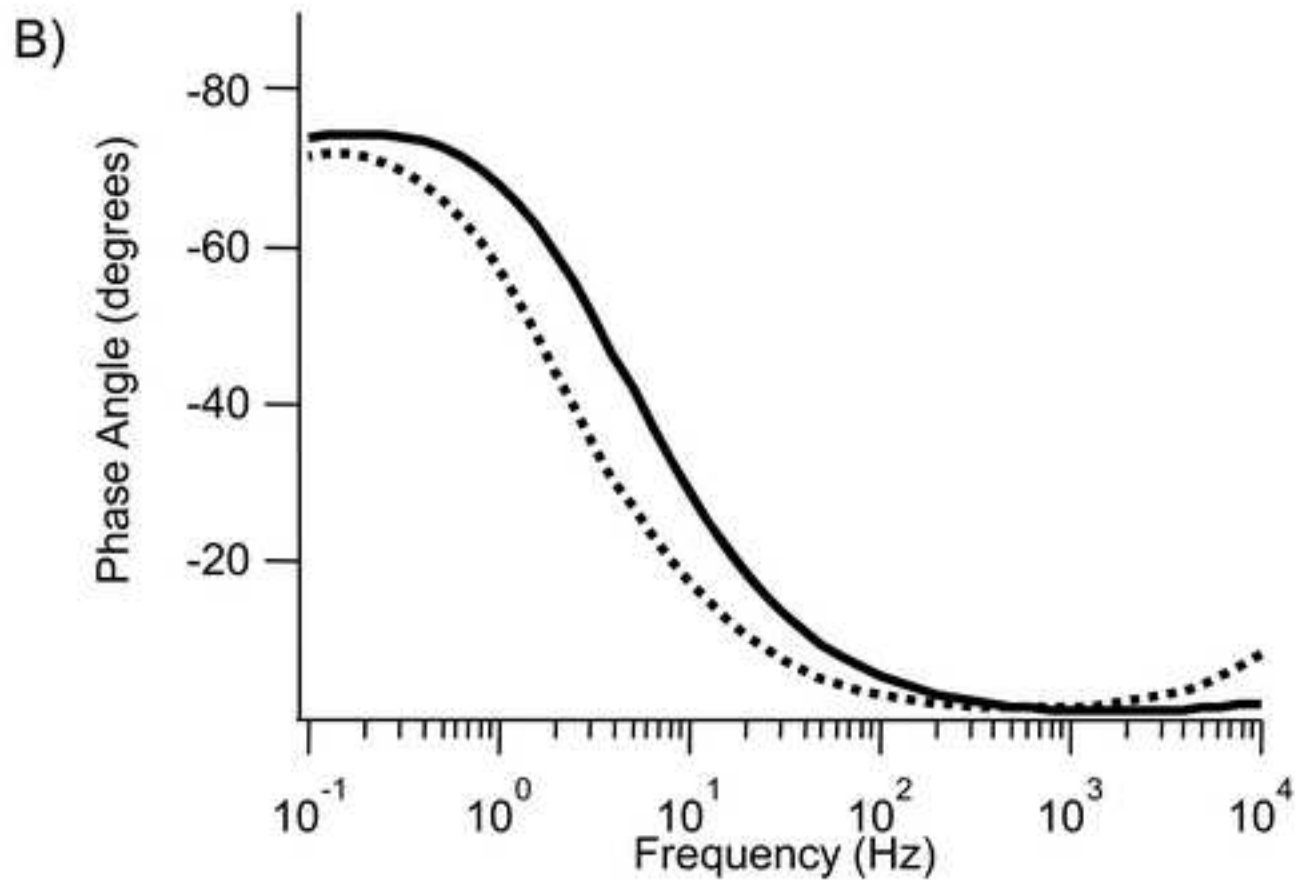
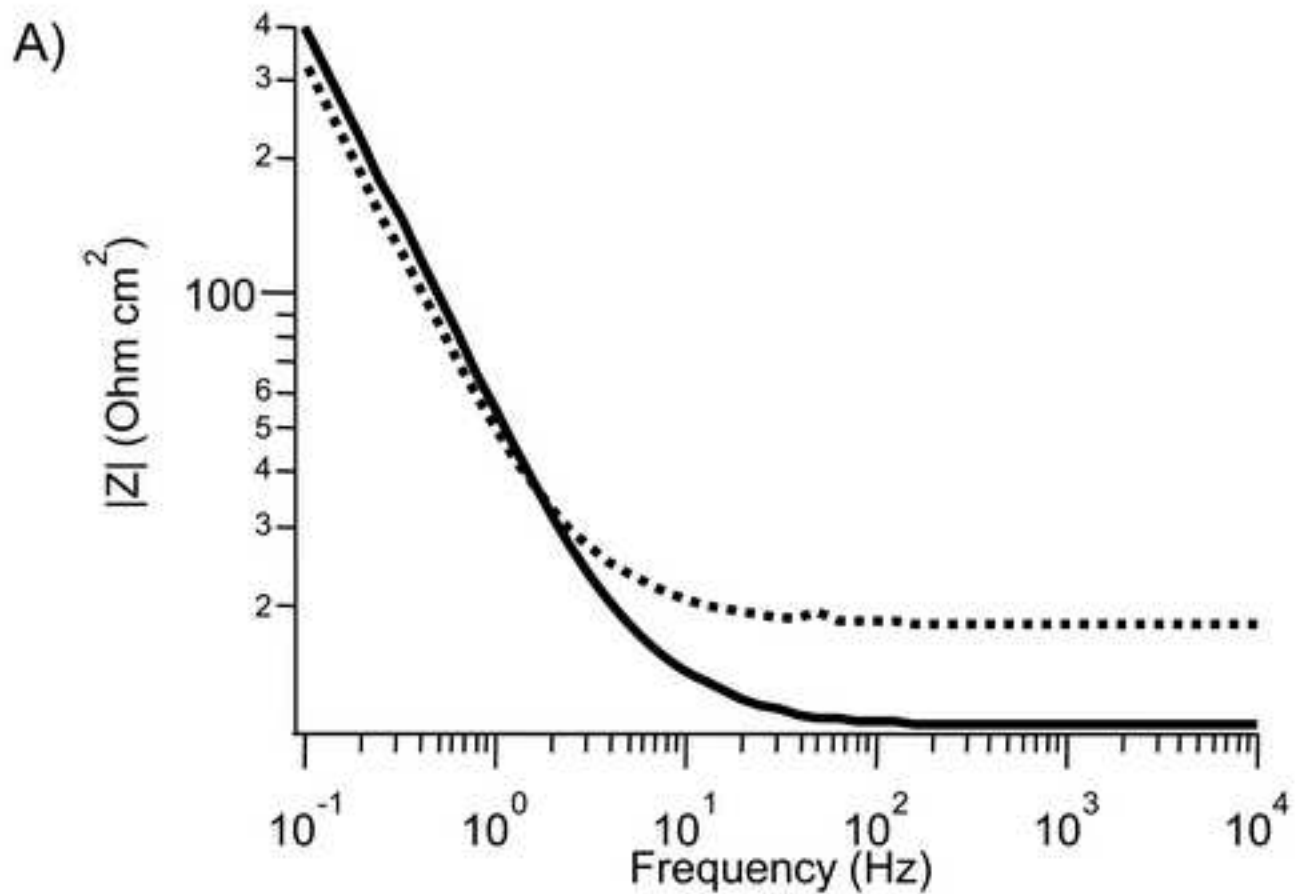


Figure 2









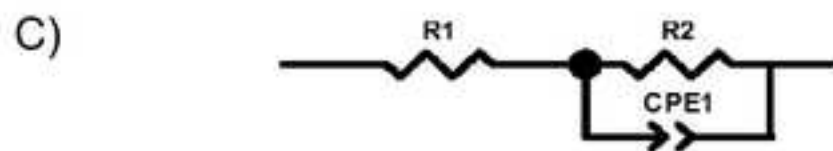
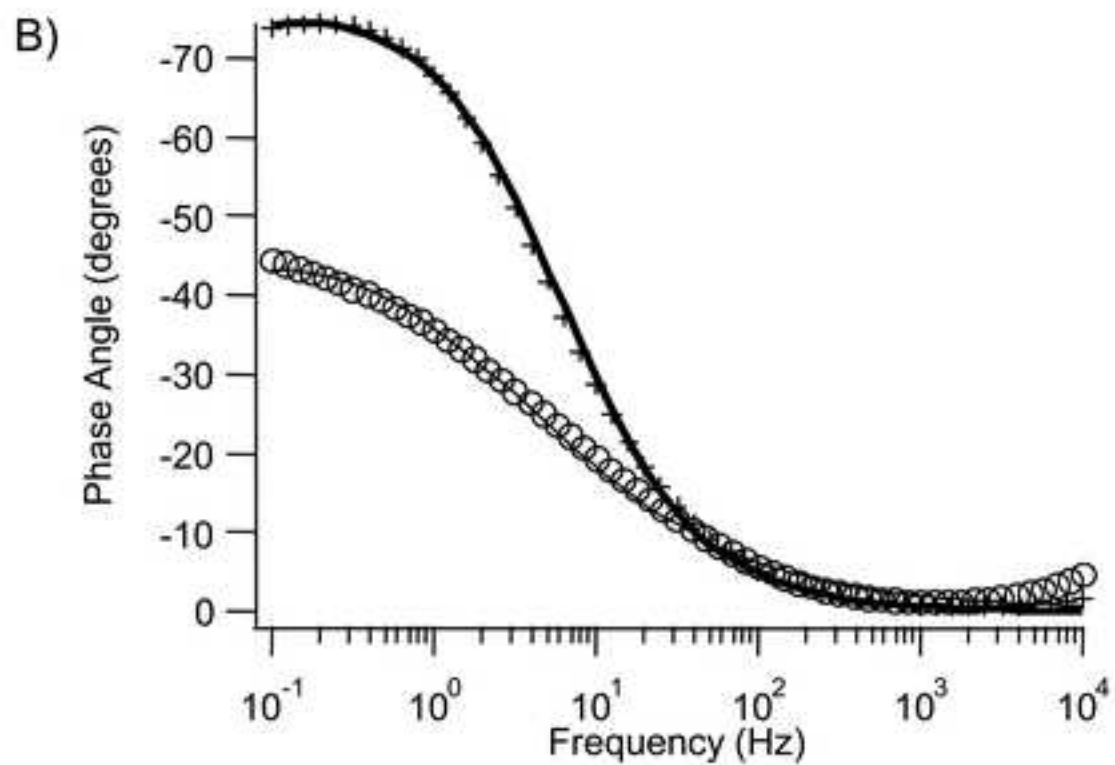
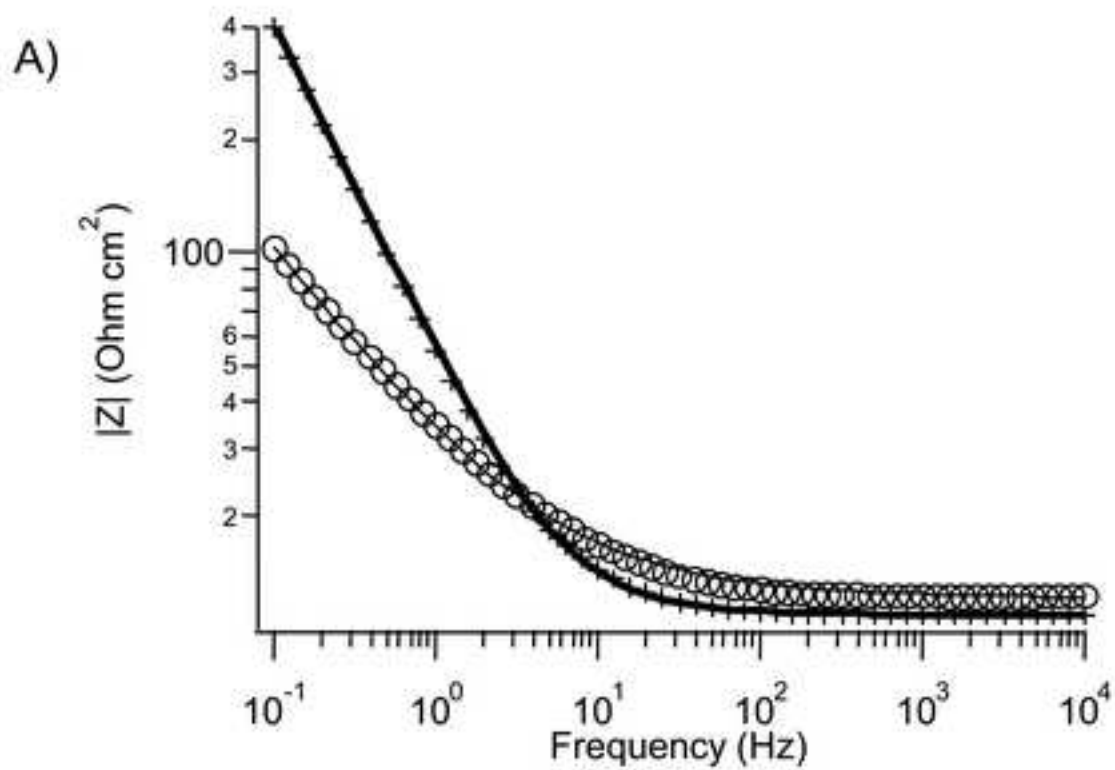


Figure 7

